Supporting Information

Bryleva et al. 10.1073/pnas.0913828107

SI Results

Effect of A1− on Cognitive Deficits of AD Mice and on Cognitive Functions of Non-AD Mice. We performed hippocampal (i.e., context)–dependent and amygdala (i.e., cued)–dependent memory tests on age-matched (2, 9, and 12 month-old) A1+/AD, A1−/AD, and NTG mice. The results show that mice of all three genotypes at different ages were able to learn equally well (Fig. S3*A*). In contextual memory testing, there was no difference among these mice at 2 months of age; at 9 and 12 months, when compared with NTG mice, the A1+/AD mice exhibited an approximate 50% deficit, whereas the A1−/AD mice exhibited no deficit (Fig. S3*B*). In cued memory tests, there was no difference among the mice at 2 months; at 9 months, when compared with NTG mice, the A1+/AD mice exhibited a trend toward a decline; however, the difference was not statistically significant. At 12 months, a statistically significant memory decline in the A1+/AD mice was observed. In contrast, the A1−/AD mice exhibited no deficit at either 9 or 12 months (Fig. S3*C*). These results indicate that A1− causes amelioration in the hippocampal- and amygdala-dependent cognitive deficits in AD mice at 9 to 12 months of age. As a control, we also performed contextual and cued memory tests on the A1+ and A1− mice in the C57BL/6 background at 9 and 12 months of age. The results showed that the A1+ and A1− mice were able to learn equally well (Fig. S3*D*); in either contextual or cued memory tests, the difference between the A1− mice and the A1+ mice was not statistically significant (Fig. S3 *E* and *F*).

SI Materials and Methods

Mice. Mice were fed ad libitum with standard chow diet, maintained in a pathogen-free environment in single-ventilated cages, and kept on a 12-h light/dark schedule, using Dartmouth Animal Research Center Institutional Animal Care and Use Committee–approved protocol number 08.05.01.

Mouse Tissue Isolation. Animals were killed by CO_2 asphyxiation. The brains, adrenals, and livers were rapidly isolated. Mouse brains were dissected into various regions on ice within 5 min and were either used fresh (for ACAT enzyme activity assay) or rapidly frozen on dry ice for other usage.

ACAT Activity Assay, IP, and Immunoblot Analyses. Freshly isolated tissue samples were homogenized on ice in 50 mM Tris, 1 mM EDTA, pH 7.8, with protease inhibitors, and then solubilized in detergent using 2.5% CHAPS and 1 M KCl. The homogenates were centrifuged at 100,000 × *g* for 45 min at 4 °C. The supernatants were used for ACAT activity assay in mixed micelles and for IP and immunoblot analyses (1, 2).

In Situ Hybridization. In situ hybridization was performed using procedures described earlier (3).

Immunohistochemical and Thioflavin S Staining. Immunohistochemistry was performed as described (4). Thioflavin S staining was according to the protocol as described (5), using free-floating sections. Confocal analysis of thioflavin S-positive amyloid deposits was performed as described (6).

Preparation of Brain Homogenates and Immunoblot Analysis of APP and Its Fragments. Brain homogenates were prepared in the sucrose buffer with protease inhibitors at 4 °C according to published protocol (7). Aliquots of homogenates were quickly frozen on dry ice and stored at −80 °C. Upon use, frozen homogenates were thawed on ice and centrifuged for 1 h at 100,000 × *g* at 4 °C; the supernatants contained soluble proteins including sAPPα and sAPPβ, whereas the pellet contained membrane-associated, insoluble proteins including full-length APP, CTFα, and CTFβ. Immunoblot analysis of APP and its fragments was according to Cheng et al. (8). The following antibodies were used: anti–human-Aβ 6E10 (1:5,000; Covance), anti–human-APP 369 antiserum (1:1,000; gift from Sam Gandy, Philadelphia, PA), monoclonal anti–HMG-CoA reductase IgG-A9 (1:3; obtained from ATCC), anti–mouse-CYP46A1 (1:125; Zymed/Invitrogen), and β-actin (1:5,000; Sigma). Densitometric analysis was performed using National Institutes of Health Image software.

Aβ Analysis by ELISA. Samples were prepared using a previously published protocol (9), loaded undiluted or diluted five to 10 fold onto the "human β amyloid (1-40)" or "human β amyloid (1-42)" ELISA plate (Wako), and analyzed according to protocol provided by Wako.

Contextual Fear Conditioning. Contextual fear conditioning was performed according to a published protocol (10), (11). The auditory cue was from http://www.e2s.com/. GoldWave software program was used to edit the auditory cue; WinAmp software was used to play the cue sound using the speakers. The digital sound level meter (RadioShack) was used to adjust the cue sound level to 87 dB. Each mouse behavior was recorded using a computer Web cam (QuickCam; Logitech) and ANY-maze recording software. The videos were analyzed for freezing behavior, using time sampling at 5-s intervals.

RNA Isolation, RT-PCR, and Real-Time PCR. Total RNA was isolated with TRIzol reagent (Invitrogen), stored at −80 °C, and used for RT-PCR experiments, using the protocol supplied by the manufacturer. Real-time PCR was performed using the DyNamo HS SYBR Green qPCR kit (New England Biolabs). Relative quantification was determined by using the ΔΔCT method (12). Mouse ACAT1 and human APP primers were designed using Oligo 4.0 Primer Analysis Software. Mouse ACAT2, neurofilament 120-kDa (NF120), and GAPDH primer sequences were previously published (13–15). The primer sequences used for Figs. 1, 3, and 5 in the main text are listed in Table S1. The PCR temp conditions for primers listed in Table S1 included an initial denaturation at 94 °C for 5 min. Subsequently, 40 cycles of amplification were performed, which included denaturation at 94 °C for 10 s, annealing at 56 °C for 20 s, and elongation at 72 °C for 29 s. The primer sequences for Fig. 4 in the main text are listed in Table S2; the PCR conditions were as previously published (16).

Sterol Composition Analysis in Mouse Brains. Mice forebrains were homogenized and extracted using chloroform:methanol (2:1; at 12 mL final volume per mouse brain), dried down under nitrogen, and redissolved in MeOH. A 10% sample was placed in a 2-mL GC/MS autosampler vial, dried down, and trimethyl-silyl derivatized overnight at room temperature with 0.5 mL Tri-Sil TBT (Pierce). One microliter of derivatized sample (or 0.1 μL for cholesterol measurements) was injected into a Shimadzu QP 2010 GC-MS instrument. GC/MS analysis of sterols was according to the method outlined (17) with modifications, using selected ion monitoring (cholesterol, 329, 353, 368, 458; desmosterol, 441; lanosterol, 393; 24SOH, 413) and standard curves for quantification.

Sterol, Fatty Acid, and Cholesterol Ester Synthesis in Mouse Brains. Sterol and fatty acid synthesis in mouse brains was measured

according to the method described (18). A similar method was developed to measure cholesterol esterification from [^{3}H]cholesterol in vivo: mice were anesthetized with ketamine xylazine (0.1 mL/30 g body weight), mounted onto the Kopf stereotaxic instrument. After sagittal skin incision, [^{3}H]cholesterol at 10 μCi/mouse prepared in 3 μL of 5 mM methyl β-cyclodextrin in PBS solution was injected into the right lateral ventricle with a glass syringe in 2 min. Mice were kept in cages for 3 h, then euthanized by CO_2 gas. The forebrains were removed; lipids were extracted and redissolved in MeOH as described earlier. Ten percent of the redissolved sample was analyzed by TLC, using plates from Analtech (no. 46911), using a solvent mixture of hexanes, ethyl ether (anhydrous), and acetic acid (60:40:1). The cholesterol and CE bands were scraped off the TLC plate and counted. Percent cholesterol esterification was determined by dividing the [^{3}H]CE count by the total [^{3}H]cholesterol count.

Sterol Synthesis and Cholesterol Esterification in Primary Neuronal Cell Culture. Hippocampal neurons were isolated from A1+/AD and A1−/AD mice at postnatal d 5 according to protocol described (19, 20). Cells were seeded in 6-well dishes in triplicates at 300,000 cells/well, and grown in 3 mL/well Neurobasal A medium with 1× B27, 0.5 mM L-Gln, and 5 ng/mL FGF for 14 d. Half the media were replaced with fresh media once every 7 d. Forty-eight h after the second media replacement, 50 μCi of [^{3}H]sodium acetate (100 mCi/mmol) in PBS solution was added per well for 3 h. Lipids in cells and in media were extracted, saponified, and analyzed by using the same TLC system described earlier. To minimize sterol oxidation, samples were protected from light and heat during lipid extraction, and were analyzed without storage. To improve separation, after sample loading, the TLC plate was placed under vacuum for 30 min before chromatography. [^{3}H]-Labeled sterol bands were identified based on iodine stainings of unlabeled sterols added to samples before lipid extraction. Rf values were as follows: lanosterol, 0.5; cholesterol, 0.38; and 24SOH, 0.2. The bands were scrapped off and counted. For each labeled sterol, the counts present in cells and in media were added to calculate the synthesis rate for that sterol. The identification of [^{3}H]24SOH was confirmed by using a different TLC system with the solvent mixture of heptane, anhydrous ether, methanol, and acetic acid at 80:35:3:2. Rf values were as follows: lanosterol, 0.36; cholesterol, 0.30; 24SOH, 0.20. An additional control experiment showed that, when administrated [^{3}H]sodium acetate, the nonneuronal cell line MCF-7 [which lacks the enzyme 24(S)-hydroxylase; CYP46A1] synthesizes an ample amount of [^{3}H]cholesterol without synthesizing detectable level of [^{3}H]24SOH. Cholesterol esterification in intact cells was conducted according to a method described earlier (21); the [^{3}H]oleate pulse time was 3 h.

1. Chang CC, et al. (1998) Recombinant acyl-CoA:cholesterol acyltransferase-1 (ACAT-1) purified to essential homogeneity utilizes cholesterol in mixed micelles or in vesicles in a highly cooperative manner. *J Biol Chem* 273:35132–35141.
2. Chang CC, et al. (2000) Immunological quantitation and localization of ACAT-1 and ACAT-2 in human liver and small intestine. *J Biol Chem* 275:28083–28092.
3. Poirier S, et al. (2008) The proprotein convertase PCSK9 induces the degradation of low density lipoprotein receptor (LDLR) and its closest family members VLDLR and ApoER2. *J Biol Chem* 283:2363–2372.
4. Oddo S, et al. (2003) Triple-transgenic model of Alzheimer's disease with plaques and tangles: intracellular Abeta and synaptic dysfunction. *Neuron* 39:409–421.
5. Guntern R, Bouras C, Hof PR, Vallet PG (1992) An improved thioflavine S method for staining neurofibrillary tangles and senile plaques in Alzheimer's disease. *Experientia* 48:8–10.
6. Dickson TC, Vickers JC (2001) The morphological phenotype of beta-amyloid plaques and associated neuritic changes in Alzheimer's disease. *Neuroscience* 105:99–107.
7. Schmidt SD, Jiang Y, Nixon RA, Mathews PM (2005) Tissue processing prior to protein analysis and amyloid-beta quantitation. *Methods Mol Biol* 299:267–278.
8. Cheng IH, et al. (2007) Accelerating amyloid-beta fibrillization reduces oligomer levels and functional deficits in Alzheimer disease mouse models. *J Biol Chem* 282:23818–23828.
9. Schmidt SD, Nixon RA, Mathews PM (2005) ELISA method for measurement of amyloid-beta levels. *Methods Mol Biol* 299:279–297.
10. Comery TA, et al. (2005) Acute gamma-secretase inhibition improves contextual fear conditioning in the Tg2576 mouse model of Alzheimer's disease. *J Neurosci* 25:8898–8902.
11. Jacobsen JS, et al. (2006) Early-onset behavioral and synaptic deficits in a mouse model of Alzheimer's disease. *Proc Natl Acad Sci USA* 103:5161–5166.
12. Pfaffl MW, Horgan GW, Dempfle L (2002) Relative expression software tool (REST) for group-wise comparison and statistical analysis of relative expression results in real-time PCR. *Nucleic Acids Res* 30:e36.
13. Sakashita N, et al. (2003) Acyl-coenzyme A:cholesterol acyltransferase 2 (ACAT2) is induced in monocyte-derived macrophages: in vivo and in vitro studies. *Lab Invest* 83:1569–1581.
14. Kuwahara C, et al. (2000) Enhanced expression of cellular prion protein gene by insulin or nerve growth factor in immortalized mouse neuronal precursor cell lines. *Biochem Biophys Res Commun* 268:763–766.
15. Pan PW, Rodriguez A, Parkkila S (2007) A systematic quantification of carbonic anhydrase transcripts in the mouse digestive system. *BMC Mol Biol* 8:22.
16. Van Eck M, et al. (2003) Differential effects of scavenger receptor BI deficiency on lipid metabolism in cells of the arterial wall and in the liver. *J Biol Chem* 278: 23699–23705.
17. Ebner MJ, Corol DI, Havlíková H, Honour JW, Fry JP (2006) Identification of neuroactive steroids and their precursors and metabolites in adult male rat brain. *Endocrinology* 147:179–190.
18. Reid PC, et al. (2008) Partial blockage of sterol biosynthesis with a squalene synthase inhibitor in early postnatal Niemann-Pick type C npcnih null mice brains reduces neuronal cholesterol accumulation, abrogates astrogliosis, but may inhibit myelin maturation. *J Neurosci Methods* 168:15–25.
19. Brewer GJ (1997) Isolation and culture of adult rat hippocampal neurons. *J Neurosci Methods* 71:143–155.
20. Price PJ, Brewer GJ (2001) *Protocols for Neural Cell Culture*, eds Fedoroff S, Richardson A (Humana Press, Inc., Totowa, NJ), pp 255–264.
21. Chang CCY, Doolittle GM, Chang TY (1986) Cycloheximide sensitivity in regulation of acyl coenzyme A:cholesterol acyltransferase activity in Chinese hamster ovary cells. 1. Effect of exogenous sterols. *Biochemistry* 25:1693–1699.
22. Chang TY, Chang CCY, Bryleva E, Rogers M, Murphy S (2010) Neuronal cholesterol esterification by ACAT1 in Alzheimer's disease. *IUBMB Life. In Press.*

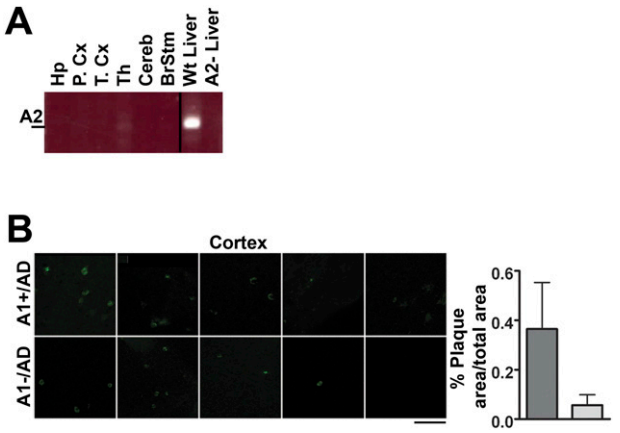

Fig. S1. (*A*) A2 mRNA in the 4-month-old WT mouse brain regions. RT-PCR analysis was performed. WT and A2− mice liver samples were used as positive and negative controls. *Hp*, hippocampus; *P. Cx*, parietal cortex; *T. Cx*, temporal cortex; *Th*, thalamus; *Cereb*, cerebellum; *BrStm*, brainstem. (B) Amyloid plaque load (using thioflavin S staining) in the cortex of 17-month-old A1−/AD mice. The difference was not statistically significant ($P = 0.172$). Data represent mean ± SEM, $n = 5$. (Scale bar: 100 μm.)

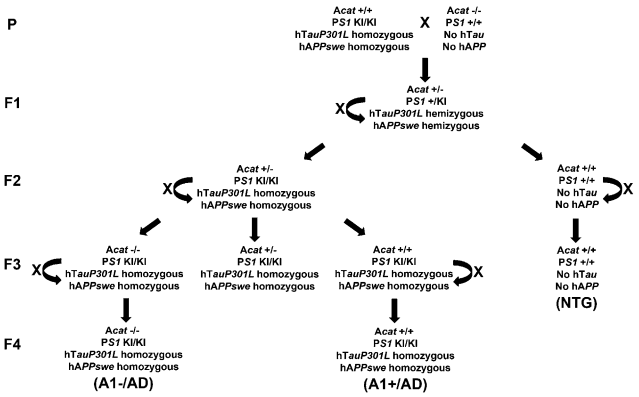

Fig. S2. Breeding strategy used to produce the paired A1−/AD and NTG mice. The 3XTg-AD mice were bred with A*cat1*$^{-/-}$ mice to obtain the F1 mice. The F1 mice were bred to each other to produce the F2 mice. The F2 mice were selected for the desirable genotype, using PCR for P*s1* and A*cat1* and Southern blot analysis for A*pp* and T*au*. The selected F2 mice, heterozygous for A*cat1*, homozygous for Ps1 knock-in (*KI*), human T*auP301L*, and human A*PPswe* transgenes, were maintained to establish a breeding colony to produce the F3 AD mice; one fourth of the F3 mice are A*cat1*$^{-/-}$, half are A*cat1*$^{+/-}$, and one fourth are A*cat1*$^{+/+}$. The paired F4 AD mice (A1−/AD and A1+/AD) were used in the current study. The NTG mice were selected from breeding of the appropriate F2 mice as indicated.

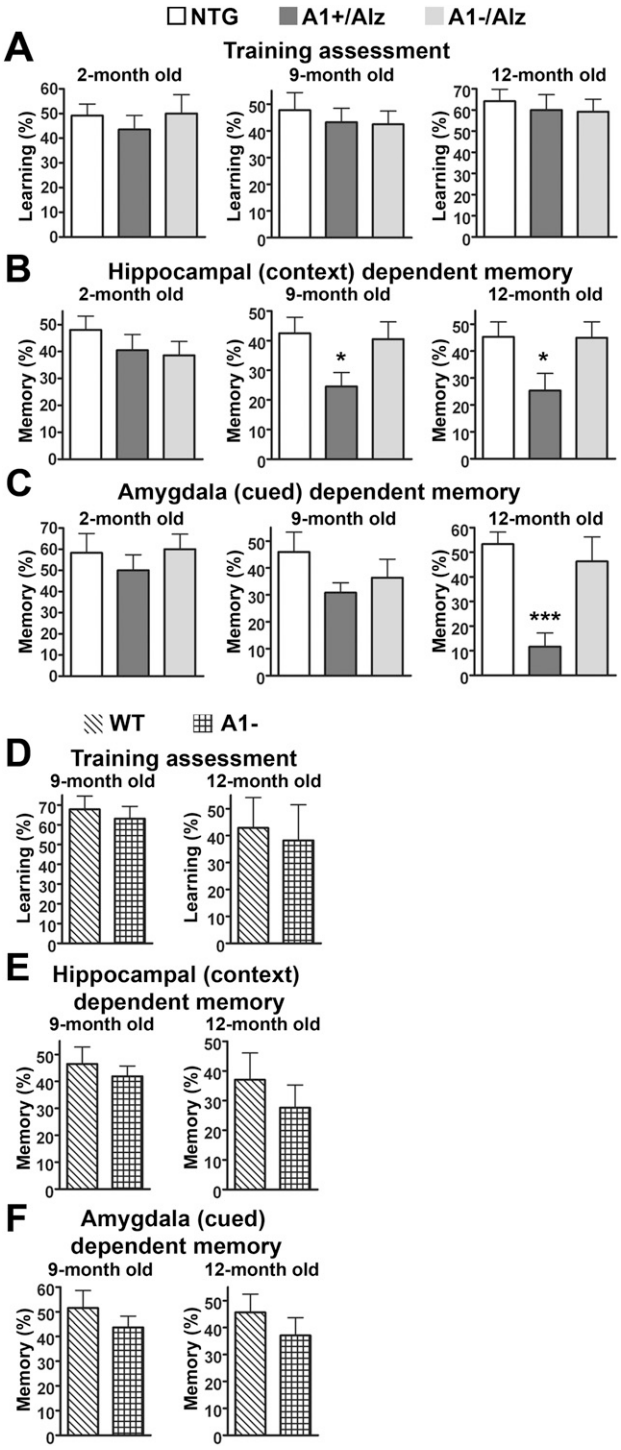

Fig. S3. (*A*) Training assessment, (*B*) hippocampal (i.e., context)–dependent memory test and (C) Amyglada (i.e., cued)–dependent memory test performed in NTG, A1+/AD, and A1−/AD mice at different ages as indicated; n = 9 for 2-month-old, n = 11 for 9-month-old, and n = 10 for 12-month-old mice of each genotype. In *B*, for 9- and 12-month-old A1+/AD mice, the difference compared with NTG was significant (P = 0.021 and P = 0.029); for A1−/AD mice compared with NTG mice, the difference was not significant (P = 0.802 and P = 0.967). In *C*, for 12-month-old A1+/AD mice, the difference compared with NTG was significant ($P < 0.0001$); for A1−/AD mice compared with NTG, the difference was not significant (P = 0.537). (*D*) Training assessment, (*E*) hippocampal-dependent memory test and (*F*) Amygdala-dependent memory assessment performed in A1+ and A1− mice in C57BL/6 background at different ages as indicated; n = 6 of each genotype. In *D*–*F*, the differences between the A1− mice and the A1+ mice were not statistically significant. Data represent mean ± SEM. *$P < 0.05$; ***$P < 0.001$.

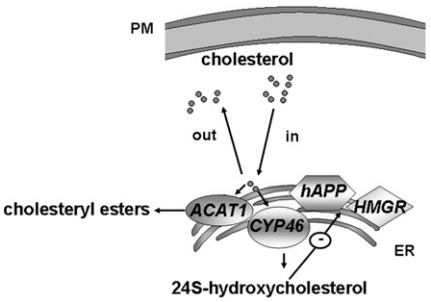

Fig. S4. A working model that links cholesterol trafficking with ACAT1, CYP46A1, 24SOH biosynthesis, hAPP, and HMGR at the ER. This model depicts that A1– increases 24SOH content by providing more cholesterol at the ER as substrate for CYP46A1. The increase in 24SOH and/or cholesterol at the ER decreases the hAPP content and HMGR protein content at the ER. See *Text* for details. Chang et al. [22] provides more elaborative discussions on CE and 24SOH contents in mouse brains, and on the roles of oxysterols in vivo.

Table S1. Primer sequences used in Figs. 1, 3, and 5 in the main text and in Fig. S1*A* in Supporting Information

Gene (sense/antisense)	Amplicon size
ACAT1	274
5′-AGCCCAGAAAAATTTCATGGACACATACAG-3′	
5′- CCCTTGTTCTGGAGGTGCTCTCAGATCTTT-3′	
ACAT2	530
5′-TTTGCTCTATGCCTGCTTCA-3′	
5′- CCATGAAGAGAAAGGTCCACA-3′	
GAPDH	186
5′-ATGGTGAAGGTCGGTGTG-3′	
5′- CATTCTCGGCCTTGACTG-3′	
NF120	382
5′-ACGGCGCTGAAGGAGATC-3′	
5′- GTCCAGGGCCATCTTGAC-3′	
Human APP	260
5′-CCCACTGATGGTAATGCTGGC-3′	
5′- GGAATCACAAAGTGGGGATGG-3′	

Table S2. Primer sequences used in Fig. 4 in the main text

Gene (sense/antisense)	Amplicon size
ABCA1	96
5′-GGTTTGGAGATGGTTATACAATAGTTGT-3′	
5′-TTCCCGGAAACGCAAGTC-3′	
ABCG1	85
5′-AGGTCTCAGCCTTCTAAAGTTCCTC-3′	
5′-TCTCTCGAAGTGAATGAAATTTATCG-3′	
ABCG4	541
5′-CTGTCCTATTCCGTGCGGGA-3′	
5′-GGGACTTCATGAGGGACACCACTT-3	
APOE	130
5′-AGCCAATAGTGGAAGACATGCA-3′	
5′-GCAGGACAGGAGAAGGATACTCAT-3′	
CYP46A1	266
5′-CAGTGAAGGTCATGCTGGAG-3′	
5′-CGCAATGAAGAAGGTGACAA-3′	
HMGR	69
5′-TCTGGCAGTCAGTGGGAACTATT-3′	
5′-CCTCGTCCTTCGATCCAATTT-3′	
HMGS	77
5′-GCCGTCAACTGGGTCGAA-3′	
5′-GCATATATAGCAATGTCTCCTGCA-3′	
HPRT	91
5′-TTGCTCGAGATGTCATGAAGGA-3′	
5′-AGCAGGTCAGCAAAGAACTTATAGC-3′	
LDLR	
5′-CTGTGGGCTCCATAGGCTATCT-‘3	68
5′-GCGGTCCAGGGTCATCTTC-3′	
LRP	
5′-TGGGTCTCCCGAAATCTGTT-3′	95
5′-ACCACCGCATTCTTGAAGGA-3′	
SREBP1	
5′-AACCAGAAGCTCAAGCAGGA-3′	121
5′-TCATGCCCTCCATAGACACA-3′	
SREBP2	
5′-GTGGAGCAGTCTCAACGTCA-3′	150
5′-TGGTAGGTCTCACCCAGGAG-3′	
SQS	
5′-CCAACTCAATGGGTCTGTTCCT-3′	137
5′-TGGCTTAGCAAAGTCTTCCAACT-3′	